Solute Trapping of Group III, IV, and V Elements in Silicon by an Aperiodic Stepwise Growth Mechanism

Solute trapping of group III, IV, and V elements in silicon by an aperiodic stepwise growth mechanism

Riccardo Reitano,[a] Patrick M. Smith,[b] and Michael J. Aziz
Division of Applied Sciences, Harvard University, 29 Oxford Street, Cambridge, Massachusetts 02138

(Received 24 February 1994; accepted for publication 25 April 1994)

With rapid solidification following pulsed laser melting, we have measured the dependence on interface orientation of the amount of solute trapping of several group III, IV, and V elements (As, Ga, Ge, In, Sb, Sn) in Si. The aperiodic stepwise growth model of Goldman and Aziz accurately fits both the velocity and orientation dependence of solute trapping of all of these solutes except Ge. The success of the model implies a ledge structure for the crystal/melt interface and a step-flow mechanism for growth from the melt. In addition, we have observed an empirical inverse correlation between the two free parameters ("diffusive speeds") in this model and the equilibrium solute partition coefficient of a system. This correlation may be used to estimate values of these free parameters for other systems in which solute trapping has not or cannot be measured. The possible microscopic origin of such a correlation is discussed.

I. INTRODUCTION

The description of solidification phenomena over a range of interface velocities several orders of magnitude wide (10^{-2}–10^{1} m/s) requires knowledge of the equilibrium solidification properties as well as how the material behaves when the departure from equilibrium becomes significant. For low solidification velocities, the description of solidification is based on the assumption that the interface is in local equilibrium; i.e., the solid and the liquid immediately adjacent to the interface can be considered to be in equilibrium with each other. In this case the concentration of solute in the liquid at the interface can be obtained using transport theory in the liquid, while the concentration in the growing crystal can be estimated from the equilibrium phase diagram. At high velocities, such as those obtained by pulsed laser melting, there is much less time for equilibration between the crystal and the melt across the interface, and the assumption of local equilibrium is no longer valid; departure from equilibrium is expected.

One readily apparent consequence of the deviations from local equilibrium in rapid solidification is the formation of a highly supersaturated solid;[1,2] in the case of pulsed laser melting of doped silicon, supersaturations by factors of up to 10^5 have been reported[3] following growth at rates of a few meters per second. Because such supersaturation implies that the chemical potential of the solute actually rises upon crystallization,[2] the process is called "solute trapping." A distinct but closely related phenomenon is the suppression of solute/solvent partitioning at the rapidly moving crystal/melt interface. This suppressed partitioning is the mechanism whereby such supersaturations are attained; as a consequence the term "solute trapping" is also used synonymously with suppressed partitioning. The partition coefficient k, the ratio of solute compositions in the solid and in the liquid at the interface, undergoes a transition from its equilibrium value k_e to unity as the growth rate increases. This has been shown to occur for many impurities in silicon.[4] The trapping process can be understood from a kinetic point of view in terms of the restricted mobility of the solute as it diffuses through the interface. When the interface velocity v approaches the maximum speed of diffusion (the "diffusive speed" v_D, given by the ratio of the solute diffusivity at the interface to the atomic jump distance), the solute atoms cannot diffuse away rapidly enough to escape from the advancing interface, resulting in solute trapping.

Some insight into these phenomena has been gained with a theoretical description of the interface and an atomistic analysis of the solidification process. Several solute trapping models qualitatively give the correct dependence of k on the solidification velocity, but it is difficult to discriminate between the models because of the large uncertainties in the available experimental data. For example, the experimental data for bismuth[5] and some theoretical curves are shown in Fig. 1. Below we briefly describe the models shown in Fig. 1.

Baker's model[6] is a continuum model for dilute solutions in which the solute is treated as if diffusing in a continuum along a steep energy gradient at an interface of width δ. The one-dimensional diffusion equation is solved in steady-state with the diffusive flux assumed proportional to the product of the local concentration and chemical potential gradient. The standard free energy for the solute is assumed to vary linearly with position, from a value of E_s in the solid, to E_i in the middle of the interface, to E_l in the liquid. The diffusivity is assumed to be independent of position, except that it takes a discontinuous jump from D_l, its value in the bulk of the liquid, to D_s, its value in the bulk of the solid at the center of the interface. The ratio of E_s to E_l is fixed by the equilibrium partition coefficient, but E_i is permitted to take any value. This model predicts the possibility of a nonmonotonic $k(v)$ curve. For example, if there is strong adsorption of solute at the interface,[7] then k can undergo a transition from k_e to a value greater than unity and then back to unity. This will occur if local equilibrium between the interface

[a]Permanent address: Dipartimento di Fisica, Università di Catania, Corso Italia 57, I-95129 Catania.
[b]Present address: Lawrence Livermore National Laboratory, Livermore, CA 94550.

 0021-8979/94/76(3)/1518/12/$6.00

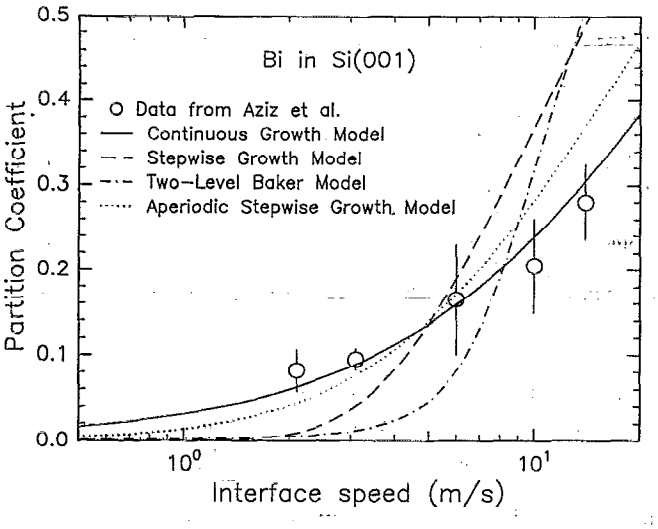

FIG. 1. Interface velocity dependence of the partition coefficient for bismuth in silicon (001). Data points are from Ref. 5; the lines are from various models as indicated.

level and the solid is lost at much lower speeds than local equilibrium between the interface level and the liquid. Whereas this behavior is physically plausible, it has never been observed experimentally. To simplify the model and reduce the number of free parameters, therefore, we have removed the energy level in the middle of the interface, resulting in the two-level Baker model.[8] We continue to require the diffusivity to remain constant throughout the interfacial region, but its value is treated as a free parameter when comparisons are made with experimental data.

In Jackson's model[9,10] chemical rate equations are written for the hopping of each species across an atomically sharp interface. The interface velocity is determined from the sum of the individual fluxes across the interface; the partition coefficient is determined from their ratio. The rate equations are not linearized. A particular form for the coupling between the fluxes of individual species is assumed. The model yields the same expression for $k(v)$ as does the continuous growth model of Aziz discussed below, but two important differences exist. (i) In the Jackson model, the maximum possible growth rate is of the order of v_D, so $k(v)$ is truncated at some $v_{\max}$ and complete solute trapping is never approached. This is in conflict with the observation of growth rates well in excess of v_D in metallic systems,[11] and with numerous observations of virtually complete solute trapping, e.g., of As in Si.[12] (ii) Because solute trapping depends on one species being less mobile than the other at the interface, if A is significantly trapped in B at some velocity, then B cannot be significantly trapped in A at any velocity. Because this result is also contrary to observation, Jackson's model[13] is not considered further below. The model fails to account for a solute atom "detaching" from a high-energy site on the solid side of the interface being by far the most likely atom to be the next to rejoin that site. This is due to stearic constraints on its diffusive escape imposed by the presence of a dense liquid.

The models of Aziz and co-workers—the continuous growth model (CGM),[8,14] stepwise growth model (SGM),[8,15] and aperiodic stepwise growth model (ASGM)[16]—are similar to Jackson's in that they use nonlinear rate equations for solute-solvent redistribution across a sharp interface. The key difference is that interface motion is treated differently from solute-solvent redistribution, as a separate reaction with a higher mobility. Crudely speaking, if the solute does nothing it ends up trapped in the solid as solvent atoms crystallize around it. In the Jackson model, if a solute atom does nothing it remains in the liquid. The growth rate in the Aziz models can exceed the diffusive speed by a large factor, and virtually complete solute trapping can occur.

The CGM treats the case when the interface is atomically rough enough that growth and redistribution occur simultaneously as strictly steady-state processes, even on the microscopic scale of the crystal lattice. It predicts a velocity-dependence of the partition coefficient given by

$$k(v)=\frac{v/v_D+k_e}{v/v_D+1}. \tag{1}$$

The SGM treats the case in which an atomically smooth, sharp interface advances by the *periodic* lateral passage of monolayer steps. The passage of a step results in the incorporation of a single liquid monolayer, including any solute atoms in the layer. Solute diffuses back into the liquid during the period before the passage of the next step, at which point any remaining solute is assumed to be permanently trapped into the solid. The predicted velocity-dependence of k for this mechanism is

$$k(v)=k_e+(1-k_e)\exp(-v_D/v). \tag{2}$$

The ASGM treats the same case as the SGM, except that the passage of steps is assumed to occur randomly, rather than periodically, in time. For a lattice in which the direction of step motion is normal to the direction of interface motion [expected to occur for the (111) interface in Si and fcc metals] the ASGM predicts, with otherwise identical boundary conditions to those in the SGM, a $k(v)$ relation identical[16] to that of the CGM, Eq. (1). Hence the ASGM for the (111) interface cannot be distinguished from the CGM by a measurement of $k(v)$ alone. Unlike the CGM, however, the ASGM can be extended to predict the orientation-dependence of k, as described below, with the addition of a second free parameter.

The two-level Baker model, the CGM, and the SGM each have only a single unknown parameter, v_D, which enters into the expression for $k(v)$ only as the ratio v/v_D. If v_D is treated as a fitting parameter and the models are plotted (see Fig. 1) on a log-velocity scale, then the only effect of a change in v_D is a rigid shift of the curve to the left or the right, without any change in shape. Figure 1 shows that the CGM fits the $k(v)$ data[17] for Si(Bi) quite well, whereas the SGM and two-level Baker model k rise too steeply with v to fit the data. The ASGM fits the data almost as well as the CGM.

In one of the first solute trapping measurements, Baeri *et al.*[18] observed a lower value for k for the (001) orientation than for the (111) at the same interface velocity in Bi-implanted silicon. An explanation based on a reduced atomic mobility resulting from greater undercooling on the (111)

than on the (100) was proposed,[19] but successful fitting requires substantially more interfacial undercooling than has been measured.[20]

The first systematic study of the orientation dependence of the partition coefficient was done by Aziz and White[21] on Bi-implanted Si; samples were cut at 5° increments from (110) through (111) to (001), so that the systematic variation of k with interface orientation could be measured. The partition coefficient at constant interface velocity was found to be sharply peaked at (111) and to decrease monotonically with increasing interface inclination from (111) [see Fig. 6(a)]. The aperiodic stepwise growth model[16] predicts this orientation dependence. It assumes that at any orientation the interface is broken into (111) terraces of single double-layer height (3.13 Å) and random width and that solidification proceeds by the lateral passage of these steps at random intervals. Some (not all, as in the SGM) of the solute atoms in the monolayer of liquid adjacent to the interface are trapped as a step passes. Because steps are expected to be atomically rough, the lateral trapping is assumed to obey CGM kinetics as a function of ledge speed. Some solute then diffuses back into the liquid through the terrace before the next layer is added, permanently covering all remaining solute. The model has two free parameters, diffusive speeds at the ledge and at the terrace (v_D^L and v_D^T, respectively). Escape through the terrace is expected to be slower than at the step edge because the solute atoms on the terrace are more highly coordinated with the crystal. The sharp peak at (111) in $k(\theta)$ occurs because as (111) is approached, the steps become more widely separated and must move faster in order to maintain a constant v imposed by heat flow. The model accounts very well for the observed velocity and orientation dependence of k of Bi in Si with only these two parameters. The ASGM expression for $k(v,\theta)$ is given by

$$k(v)=\frac{k_e+\beta_t(\beta_l+k_e)/(\beta_l+1)}{\beta_t+1}, \tag{3}$$

where $\beta_t=v/[v_D^T\cos(\theta)]$ and $\beta_l=v/[v_D^L\sin(\theta)]$; θ is the angle of inclination from (111). Reasonable numerical values of v_D^T and v_D^L are obtained from a fit of the orientation dependence Si-Bi data (see Table III). The model has also been shown to reproduce fairly well the velocity dependence of the partition coefficient for Bi[16] in (001) Si (see Fig. 1) and for As[12] in polycrystalline Si.

One problem with the ASGM is that it is doubtful that a physical experiment could ever be designed to obtain an independent measurement of the quantities treated as free parameters in the model: the speeds of atomic diffusion across a crystal/melt interface. Molecular dynamics simulations have had some success in this regard. Calculations by Cook and Clancy[22] for a rough-interface (Lennard–Jones) system have confirmed the underlying hypothesis of the continuous growth model, namely that the solute diffusion coefficient at the interface is related to the growth rate at the center of the transition from local equilibrium to complete solute trapping. Even with molecular dynamics, however, it would be extraordinarily difficult to determine separately the terrace and ledge diffusivities in a faceting system. It is also unclear how to predict diffusive speeds from first principles, or how even to make an "educated guess" for diffusive speeds in alloy systems where they have not been or cannot be measured. The best that might be hoped for is the discovery of a correlation between the diffusive speeds that fit the partitioning behavior and some other readily-measurable physical property of the alloy system.

In this work we present a systematic study of the orientation dependence of the partition coefficient for several group III, IV, and V elements in silicon. The objective of the work is to determine whether the ASGM is of general validity and, if so, to gain some insight into the relation between v_D^L, v_D^T, and other material properties.

TABLE I. Ion implantation parameters.

Ion species	Energy (keV)	Dose (cm^{-2})	Substrate temperature (K)	Amorphous thickness (nm)
Gallium	180	1.0×10^{15}	300	200
Indium	180	1.0×10^{15}	300	150
Tin	100	3.0×10^{15}	77	130
Arsenic	100	1.0×10^{16}	77	140
Antimony	100	2.5×10^{15}	77	100
Germanium	150	3.0×10^{15}	77	170

II. EXPERIMENT

Float-zoned Si wafers were cut at several inclination angles from (111) toward (001) and (110). Six different impurities (In, Sn, Sb, Ga, Ge, and As) were ion-implanted at energies and doses detailed in Table I. Rutherford backscattering spectrometry (RBS) was used to measure the implanted depth profile and the thickness of the amorphous layer resulting from implantation.

The samples were then irradiated with a pulsed XeCl excimer laser [wavelength 308 nm, pulse duration of 30 ns full width half maximum (FWHM)] at an energy high enough to melt through the entire amorphous layer and allow liquid phase epitaxial crystallization. The laser beam was passed through a homogenizer which produced a spatial uniformity of ±2% over a 2-mm-sq beam spot. Time-resolved reflectivity (TRR) measurements were performed during each shot in order to measure the melt duration; a fast digitizing oscilloscope was used to measure the intensity of a low-power argon ion laser beam reflected from the surface of the sample with a time resolution of approximately 1 ns. The laser pulse energy was calibrated by comparing the melt durations measured on a pure silicon single crystal sample with the results of heat-flow simulations.[23] In the case of As-, Ge-, and Sb-implanted samples, the back surface was heated with a high power CO_2 laser for several seconds; this reduced the interface velocity during solidification by more than an order of magnitude, as will be discussed later in detail. A schematic drawing of the experimental configuration is shown in Fig. 2. The laser irradiation parameters are listed in Table II.

The diffused impurity profile after irradiation was measured by grazing-exit RBS to enhance depth resolution. Numerical solutions to the diffusion equation were used to determine values of the partition coefficient by comparing the

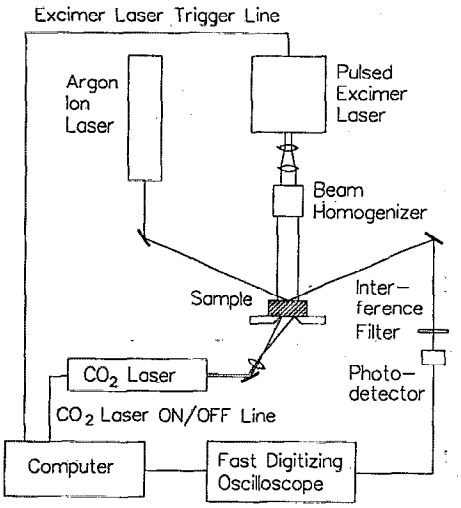

FIG. 2. Schematic drawing of the experimental setup.

experimental impurity profile with the results of the simulations. Details on the procedure are presented below.

III. RESULTS

In analyzing our data we used computer simulations of pulsed-laser induced melting and resolidification and of impurity diffusion in the liquid. In the next two subsections we will describe briefly the information extracted from these simulations.

A. Laser irradiations and heat-flow simulations

The irradiation conditions were chosen depending on the partitioning behavior of each impurity. In order to determine a value for k we required a detectable amount of surface impurity accumulation. It has been observed, for example, that about 40% of the In atoms segregate to the surface for an interface velocity of 5 m/s,[25] while until now no one has measured the partition coefficients for As in Si because of the extremely small amount of surface accumulation due to its high k value.[12]

For three of the six impurities (Ga, In, and Sn) irradiation of the samples at room temperature with a pulse energy density of 1.5 J/cm^2 (1.2 J/cm^2 for In) produced a measurable surface accumulation of the impurity. The energy density of each shot was checked by comparing the measured melt duration with that calculated by computer simulations. The simulation was performed with a numerical solution of the 1-D heat diffusion equation using the well-established optical and thermal parameters of crystalline, amorphous, and liquid Si. It has been shown that these parameters are known with sufficient accuracy to give quite good agreement between experiment and calculations for room-temperature substrates.[24] Agreement between the melt durations predicted by the simulations and the ones measured experimentally was of the order of a few percent, while the reproducibility of the laser output was about ±2%. The melt depth versus time profile calculated by the simulations was used as input to the diffusion simulations and was used to determine the solidification velocity. The average velocity was slightly different for the three impurities listed above due to differences in the thicknesses of the amorphous layers produced during implantation of the impurities prior to irradiation. The thickness of the amorphous layer was determined to be independent of orientation by RBS and ion channeling; it has been checked for all the substrate orientations for indium implantation and only for (111) and (001) for Ga and Sn implantations.

TABLE II. Laser irradiation parameters.

Ion species	Fluence (J/cm^2)	Substrate temperature (K)	Solidification velocity (m/s)
Gallium	1.5	300	4.3
Indium	1.2	300	4.5
Tin	1.5	300	4.2
Arsenic	1.0	1300–1500	0.1–0.4
Antimony	1.0	1350–1420	0.17–0.28
Germanium	1.0	1270–1450	0.13–0.61

For the other three impurities (Ge, As, and Sb) regrowth velocities of a few meters per second produced immeasurably small surface accumulation on room-temperature substrates. However, by heating the substrate with a cw-mode CO_2 laser ($\lambda = 10.6$ μm) for several seconds prior to the pulsed laser melting, we were able to obtain solidification at much slower speeds; heating times of 8 to 10 s were used to allow heat to diffuse uniformly throughout the sample. The uniformity of CO_2 heating at the moment of pulsed excimer laser melting was checked by measuring the melt duration simultaneously in the center of the sample and other points within the 2 mm×2 mm area of the sample. Using the simulated dependence of melt duration on substrate temperature described below, we determined that throughout this area the maximum temperature variation was approximately ±3%.

The excimer pulse was synchronized with the end of the CO_2 heating time, and the actual substrate temperature at which the sample was shot was estimated using heat flow simulations that determined the dependence of the melt duration, for the measured excimer pulse energy density, on substrate temperature. Melt durations scattered throughout the range 800–3200 ns were obtained, which correspond to a temperature range of 1300–1500 K for a 1 J/cm^2 pulse. The corresponding calculated average velocities were in the range 0.1–0.6 m/s. This large shot-to-shot variation in the substrate temperature was found to be unavoidable; we believe it to be due in part to variations in the output of the CO_2 laser and to differences from sample to sample in the thermal contact between the sample and the sample holder. Because k is a strong function of both orientation and solidification velocity, for a study of the orientation dependence of k it was necessary to scale to a single interface velocity the partition coefficients obtained at different velocities, as discussed below.

Finally, several samples were heated solely with the CO_2 laser (without any excimer laser pulse) and air-cooled, to determine whether the initial impurity depth profile prior to pulsed laser melting was altered by the CO_2 heating technique.

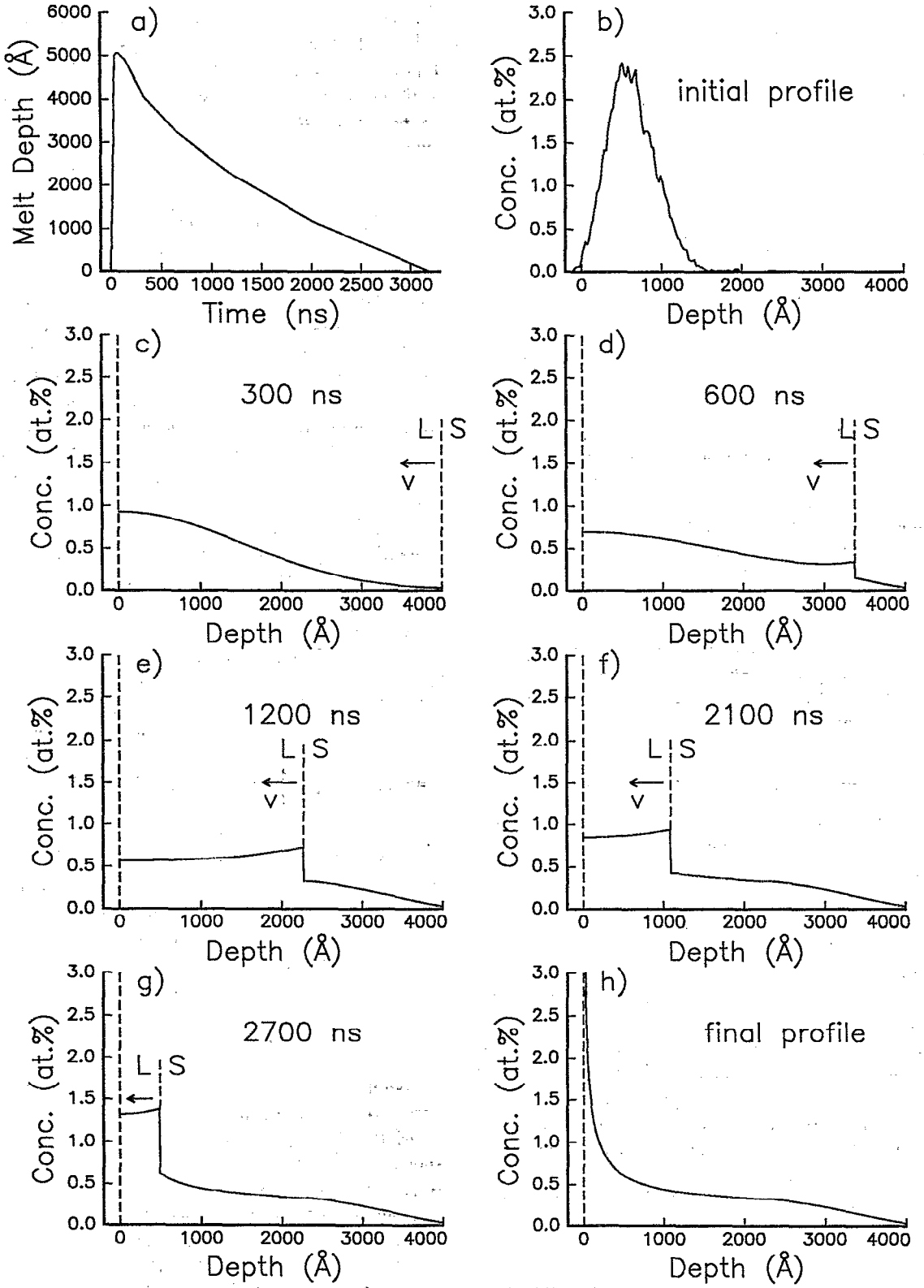

FIG. 3. (a) Calculated melt depth *vs* time profile for a 1 J/cm^2 pulse at a substrate temperature of 1500 K; (b) starting impurity profile for the diffusion simulation; (c)–(h) calculated impurity profiles at several times after the excimer pulse as indicated.

B. Diffusion simulations

The heat-flow simulations predict the interface position or melt depth (ignoring the volume decrease upon melting), as a function of time. The result of a typical simulation is shown in Fig. 3(a) for a 1 J/cm^2 pulse at a substrate temperature of 1500 K. The maximum melt depth is about 5000 Å, the melt duration is 3200 ns, and the average solidification velocity is 0.1 m/s. Melt-depth profiles such as this are cal-

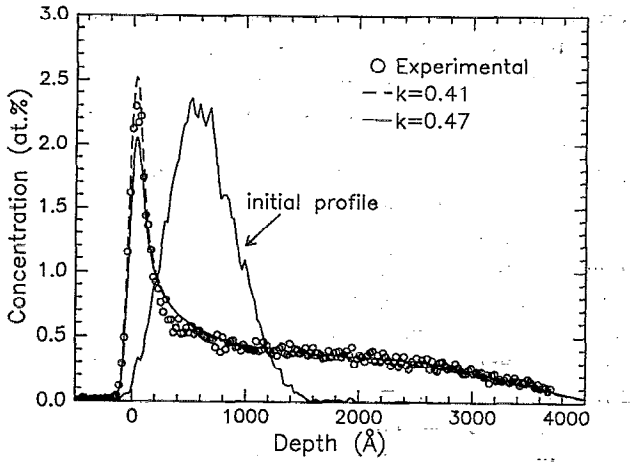

FIG. 4. Initial and diffused (circles) arsenic profiles for a (001) implanted sample. Dashed and solid lines are the calculated profiles for $D_l=3\times10^4$ cm^2/s and $k=0.41$ and 0.47, respectively; the former gives too large a surface peak while for $k=0.47$ the surface peak is too small. Our best-fit value in this case is $k=0.44$.

culated for each shot, and, together with the measured initial impurity depth profile, are used as input in the diffusion simulations. The program solves the one-dimensional diffusion equation, assuming the impurity diffuses only in the liquid. The boundary condition at the solid-liquid interface is that the ratio of solute concentration in the solid and liquid across the interface be k. This is the same simulation program used in the past to determine partition coefficients.[17] While we neglected the velocity dependence of the partition coefficient as the velocity slows down during solidification in any particular sample, this is not as crude an approximation as it may at first appear. In fact the velocity varies only slightly as the interface moves through the implanted region, especially for the high-temperature irradiations; the difference between calculations with constant k and those allowing a velocity dependence is quite small. We believe this is a negligible source of error in our analysis; good agreement between the simulated and measured impurity depth profiles, even in the tail region, confirms this. In Figs. 3(b)–3(h) the solute profile at several different times is shown, and the progressive accumulation of solute ahead of the interface is evident. When the interface returns to the free surface, the segregated solute forms a sharp surface peak; this profile must be convolved with the RBS detector resolution function in order to allow comparison with the experimental profile. In Fig. 4 the As profile for a (001) sample before and after irradiation is shown as an example; the simulated profiles were calculated using $D_l=3\times10^{-4}$ cm^2/s, $k=0.41$ (dashed line) or $k=0.47$ (solid line), and the melt depth profile shown in Fig. 3(a); in this case the best-fit (see below) value of k is 0.44.

Because we fit an entire curve and not just a single point, the fitting procedure uniquely determines not only a best-fit value of k but also a best-fit value of the liquid diffusion coefficient D_l if the latter is allowed to vary. Because the value of D_l used influences the best-fit value of k somewhat, we used the value of D_l that gives the best agreement with our data. The sensitivity of the best-fit value of k to the value of D_l used is not excessive, but uncertainties in D_l do contribute to the total uncertainty in k. Comparison will be made to literature values for D_l where the latter exist.

C. Fitting procedure

We used two different criteria to determine the "best-fit" values of k and D_l. The first was the standard least-squares fitting method. With D_l fixed at a reasonable value, the partition coefficient was varied in steps of 0.01, and the standard deviation (σ) between measured and simulated depth profiles was calculated point by point; a parabola was fit to the $\sigma(k)$ points, and the minimum of the parabola was chosen as the best-fit k for that D_l. The liquid diffusivity was then varied and the procedure repeated again; the best-fit values of D_l and k were those corresponding to the absolute minimum of σ.

An alternative method is, we believe, less susceptible to systematic errors.[26] A systematic error such as a potentially inaccurate melt depth simulation at large depths might skew the results determined solely by a least-squares fit. The alternative method is based on the steady state limit, in which the area under the surface peak is given by

$$A=C_s\left(\frac{1}{k}-1\right)\frac{D_l}{v}, \tag{4}$$

where C_s is the concentration of the growing solid. (Note that Fig. 3 represents a worst case for the steady-state hypothesis, as this is the slowest velocity used in the entire study, corresponding to the largest D_l/v width, 30 nm, of the diffusive boundary-layer.) Keeping D_l fixed, we compared the ratio A/C_S after solidification for the data and for the *fully nonsteady-state* simulations. The value of k for which this ratio for the simulated profile matches that for the measured profile is selected. Again, D_l was varied within a reasonable range (as determined by the overall fitting of the profile) to estimate the size of errors in k that this procedure could introduce. The error bars reported for values of k contain estimates of this error and that from approximately a $\pm10\%$ uncertainty in the velocity extracted from the heat-flow simulations. The final results reported here were obtained using the second fitting method. In general, the agreement of the two methods was within the reported error bars. In the few cases where the discrepancies were significant, we believe the second method to be more accurate.

D. Room temperature irradiations: Ga, In, and Sn

The irradiations of the Ga-, In-, and Sn-implanted samples were performed with the substrate held at room temperature. The regrowth velocities were between 4.2 and 4.5 m/s, depending on the amorphous layer thickness (these reported velocities are the average velocity over the last 2000 Å of growth in the simulations).

1. Gallium

In Fig. 5 we show Ga profiles for three different substrate orientations after solidification. An accumulation peak at the surface due to the zone refining effect is evident; the

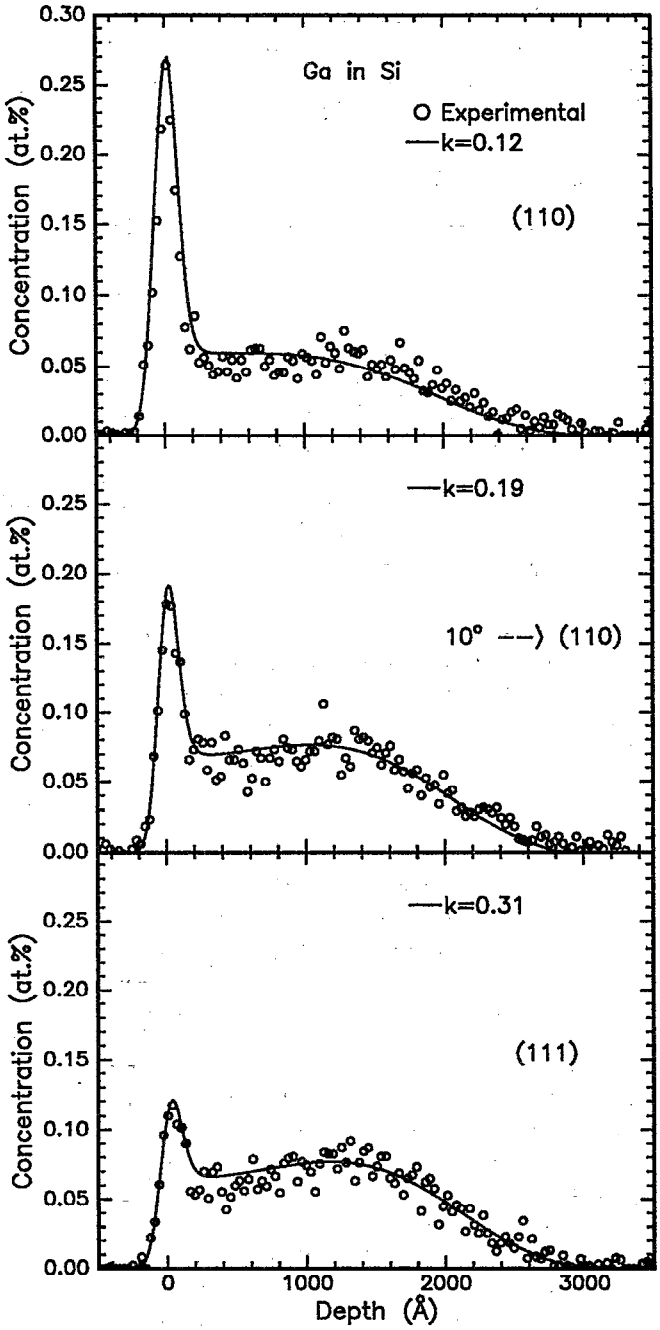

FIG. 5. Gallium profiles for three different substrate orientations. The lines are the calculated profiles for the k values indicated; circles are the experimental profiles.

finite width of the peak is due to the RBS detector resolution (12 keV). The area under the peak is much smaller for the (111) sample than for the other two, indicating a strong orientation dependence for k. The solid lines are the curves calculated with $D_l=4.8\times10^{-4}$ cm^2/s and $k=0.12$, 0.19, and 0.30 for (110), 10° off (111) toward (110) and (111), respectively. The quality of the fit is good, and the contribution to the error in k from fitting of the surface peak is estimated to be ±0.02; errors from the uncertainty in D_l will add to this value. The diffusion coefficient used is the one reported in the literature[27] (see Table III); while values of D_l a few percent above this make the fit to the depth profiles much worse, values up to 25% less than this yield acceptable fits.

The results of the analysis for all the orientations are summarized in Fig. 6(c). The partition coefficient is sharply peaked at (111), decreasing as the (110) and (001) directions are approached. The solid line is Eq. (3) fit to the data, with two free parameters, v_D^L and v_D^T. The value of v_D^T is determined by the value of k at the (111) orientation, which is independent of the value of v_D^L in the ASGM. Once v_D^T is determined, v_D^L is then varied to fit the rest of the data points. The fit is very good, and the values of the parameters are $v_D^T=10$ m/s and $v_D^L=17$ m/s. The uncertainties in D_l reported above could produce a possible reduction of v_D^T by 10%, and of v_D^L by 15%; these can be taken as typical uncertainties in v_D^T and v_D^L. In Table III the parameters for all the impurities are summarized.

2. Indium

In Fig. 6(b) the orientation dependence for In is shown. The liquid diffusion coefficient in this case is $D_l=4\times10^{-4}$ cm^2/s, which is significantly smaller than the value reported by Kodera.[27] Using Kodera's value is not possible in this case because it would predict diffusion of the impurity to depths of about 2500 Å, while the experimental profile extends only to 1800 Å. The reason for this discrepancy is not clear to us. This is the only case of significant disagreement between our values and those in the literature.

In the (110) and (001) samples the occurrence of interfacial breakdown in the near surface region was evident from the RBS spectra in the channeling condition. As a consequence, we could not fit the entire profile and ignored the fit in the top 700 Å in the analysis. The result in this case turns out to be more sensitive than normal to any variation of D_l, but once D_l is determined the accuracy is about the same. Whether or not the results of the partial fits are credible, excluding these two orientations from the fit does not change the results for v_D^T and v_D^L appreciably. We found values for v_D^T and v_D^L of 12 and 36 m/s, respectively.

3. Tin

Figure 6(d) shows the results for Sn. k is everywhere higher than in the previous two cases (Ga and In), and consequently we would expect lower v_D^T and v_D^L; in fact we found 5 m/s for v_D^T and 7 m/s for v_D^L. The best fit value for D_l was 2.5×10^{-4} cm^2/s, in excellent agreement with the value found by Hoglund *et al.*[28] in a similar experiment using (001) Si-on-sapphire samples. Our value of k for that orientation at 4.2 m/s also agrees with the value in Ref. 28. Furthermore, comparison of the $k(v)$ data of Ref. 28 for Sn in (001) Si with the $k(v)$ prediction of the ASGM for the (001) orientation, using the values of v_D^L and v_D^T from Fig. 6(d), yields good agreement comparable to that shown in Fig. 1.

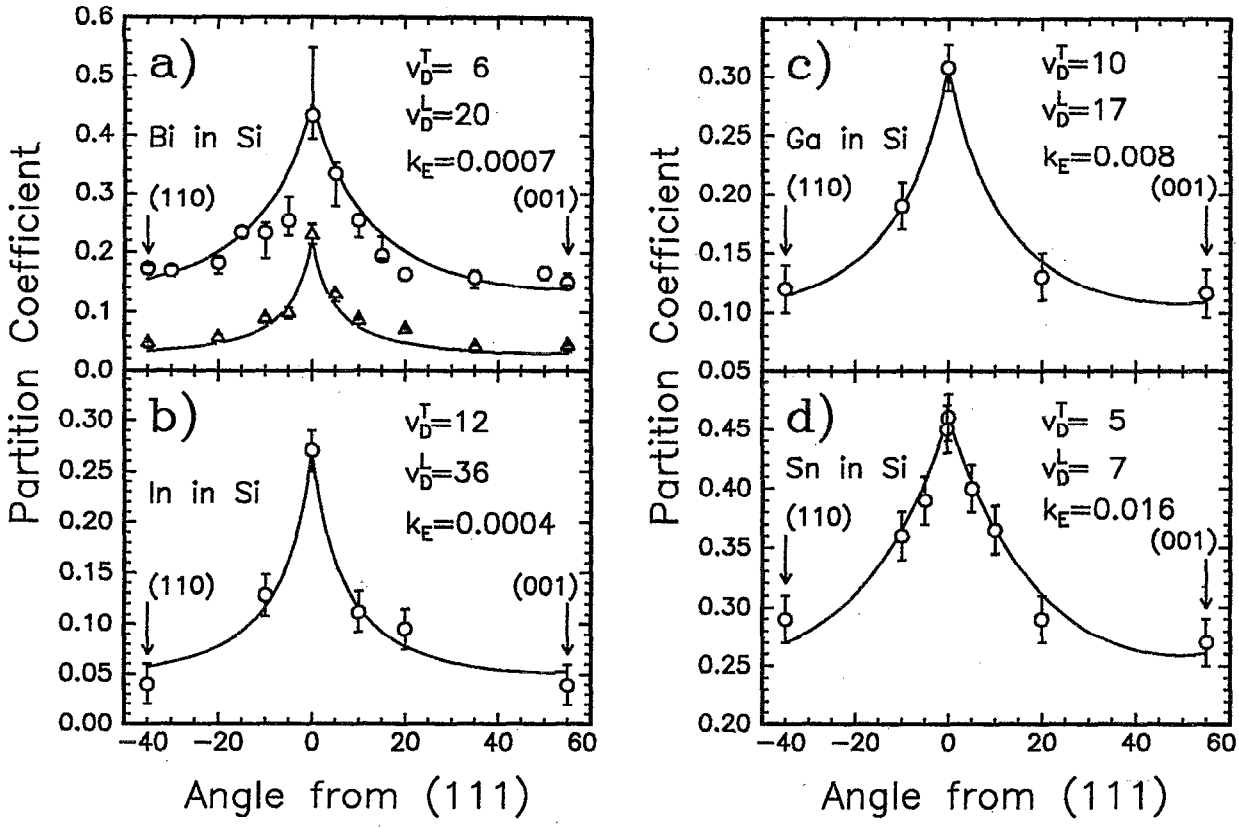

FIG. 6. Dependence of the partition coefficient on substrate orientation for (a) Bi, from Goldman and Aziz (see Ref. 16) (the circles are data taken at $v=5.0$ m/s, and the triangles are data for 1.7 m/s); (b)–(d) In, Ga, and Sn (this study, room temperature substrate, $v=4.5$, 4.3, and 4.2 m/s, respectively). The solid lines are calculated using Eq. (3) with the values of v_D^T, v_D^L, and k_e indicated.

E. High temperature irradiations: As, Sb, and Ge

1. Arsenic

TRR measurements on the pre-heated arsenic-implanted samples indicated melt durations ranging from 800 to 3200 ns. Comparison with heat-flow simulations indicates that for the measured excimer pulse energy (1.0 J/cm^2), this range of melt durations corresponds to substrate temperatures ranging from 1300 to 1500 K. At such high substrate temperatures we expect complete regrowth of the implantation-induced surface amorphous layer during the heating prior to the excimer pulse. To investigate this possibility, we analyzed similar samples which were subjected to the same heating procedure, but were not irradiated with the excimer laser pulse. Using ion channeling we concluded that the CO_2 laser completely crystallizes the amorphous layer for all substrate orientations. The minimum yield was 3%–4%, comparable to that of a virgin Si single crystal, indicating that growth occurred by solid phase epitaxy and that few, if any, dislocations or other extended defects were introduced during regrowth. The only exception was the (111) sample, for which an increase in the minimum yield to about 10% was measured. We expect that such a small change does not influence the thermal and optical properties of the material significantly, particularly for the UV pulse from the excimer laser.

TABLE III. ASGM parameters.

Ion species	k_e	D_l (10^{-4} cm^2/s)	$D_l^{\text{literature}}$ (10^{-4} cm^2/s)	v_D^T (m/s)	v_D^L (m/s)
Gallium	8×10^{-3}	4.8	4.8[a]	10	17
Indium	4×10^{-4}	4.0	6.9[a]	12	36
Tin	0.016	2.5	2.5[b]	5	7
Arsenic	0.3	3.0	3.3[a]	0.04	0.73
Antimony	0.023	2.0	1.5[a]	0.43	0.64
Germanium	0.33	3.0	4.0[c]	---	---
Bismuth[d]	7×10^{-4}	2.0	1.5[e]	6	20

[a]From Ref. 27.
[b]From Ref. 28.
[c]From Ref. 32.
[d]Data from Ref. 16.
[e]From Ref. 33.

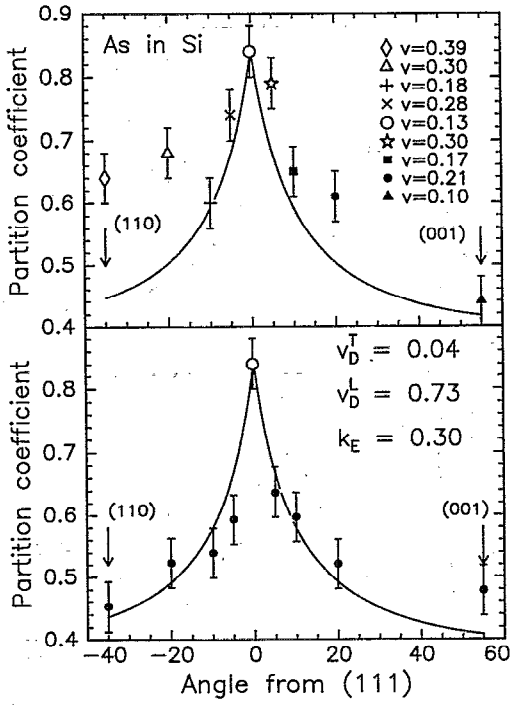

FIG. 7. Upper: Experimental data for the partition coefficient for As at various substrate orientations; note that each sample has solidified at a different interface velocity. Lower: same as before after scaling all points to $v=0.13$ m/s. The solid line is calculated from Eq. (3) with the values of v_D^T, v_D^L and k_e indicated.

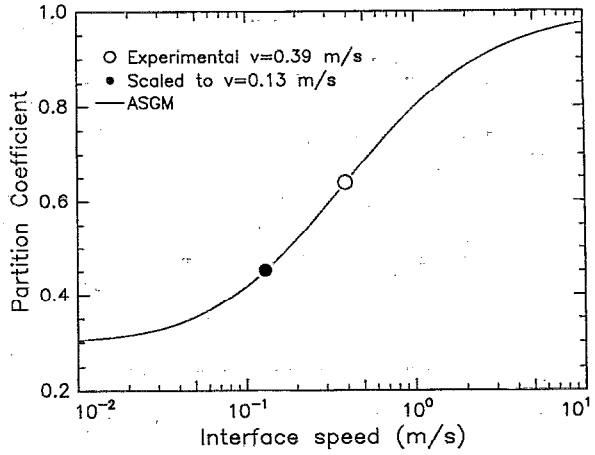

FIG. 8. Example of the scaling procedure for arsenic in silicon (110). The open circle is the measured value at $v=0.39$ m/s; the full circle represents the value of the partition coefficient scaled to a velocity of 0.13 m/s as predicted by the ASGM (dashed line).

A check on the location of the implanted impurities showed that the atoms were in substitutional sites after crystallization of the amorphous layer, but that they had diffused a very slight amount in the solid phase. The diffused profile was used as the starting profile in the diffusion simulations of melting and solidification.

Once the substrate temperature was determined by fitting heat-flow simulations to the measured melt duration, we were able to obtain very good fits of the impurity profiles resulting from melting and solidification (see Fig. 4). The "best-fit" value of D_l was 3×10^{-4} cm^2/s, in excellent agreement with the literature value.[27] Because the substrate temperature is not measured directly, it is difficult to quote a quantitative figure for the accuracy of the k values obtained by this fitting procedure. However, because the thermal and optical parameters of crystalline Si as functions of temperature are well known, we believe the accuracy of the results to be not too much worse than for those obtained from room temperature irradiation.

In the upper part of Fig. 7 the actual partition coefficients determined from the fits are shown for the arsenic-implanted samples; although k is still largest at (111) and decreases for increasing inclination angle, the points are somewhat scattered. This scatter is due to shot-to-shot variations in the solidification velocity, which varied by as much as a factor of 4, as indicated in the figure. Due to the velocity dependence of the partition coefficient we cannot compare the various k values directly. In order to fit the predicted orientation dependence of the ASGM to these data, we scaled the measured partition coefficients all to a single velocity using an iterative procedure. The following scaling method was used: (1) Because the value of k for the (111) orientation depends only on v_D^T and not on v_D^L, v_D^T was determined by fitting the data point at (111). The velocity at which this sample solidified is referred to as v_{111}. (2) For each sample i (which has a fixed orientation θ_i, velocity v_i, and measured k_i), $v_{D_i}^L$ was determined by fitting the ASGM to k_i while holding v_D^T fixed at its value determined above. (3) The value of the partition coefficient that would be expected if the sample had solidified at velocity v_{111} can now be calculated using the ASGM expression for $k(v,\theta,v_D^T,v_D^L)$:

$$k_{i,\text{scaled}}=k(v_{111};\theta_i,v_D^T,v_{D,i}^L). \tag{5}$$

This is called the "scaled" value of k. In Fig. 8 the velocity dependence predicted by the ASGM is shown for the (110) samples to illustrate this procedure. (4) The scaled partition coefficients now all correspond to the same solidification velocity, and can be fit with the ASGM's expression for $k(\theta)$ to determine an "average" or best-fit v_D^L and v_D^T. After scaling the data shown in Fig. 7(a) to a velocity of 0.13 m/s [that of the (111) sample], the scatter is markedly reduced. The data points are moved up if the experimental interface velocity was lower than 0.13 m/s and down if the velocity was higher than 0.13 m/s; the greater the velocity difference the more a point is displaced. In Fig. 7(b) the rescaled values are shown; k is 0.85 at (111) and rapidly decreases to 0.61 at 5° toward (110), and to 0.47 at (110). The fit of the orientation dependence is very good; we obtained $v_D^T=0.04$ m/s and $v_D^L=0.73$ m/s. (5) With these best-fit values of v_D^L and v_D^T, the original k_i can be rescaled to yield a second-iteration value of $k_{i,\text{scaled}}$. A new fit of the ASGM at this juncture yields new best-fit values of v_D^L and v_D^T. When the scaling of the original data [Fig. 7(a)] using these new values of v_D^T and v_D^L produces new corrected points very close to the previous ones, as in this case, iteration of the procedure is not necessary.

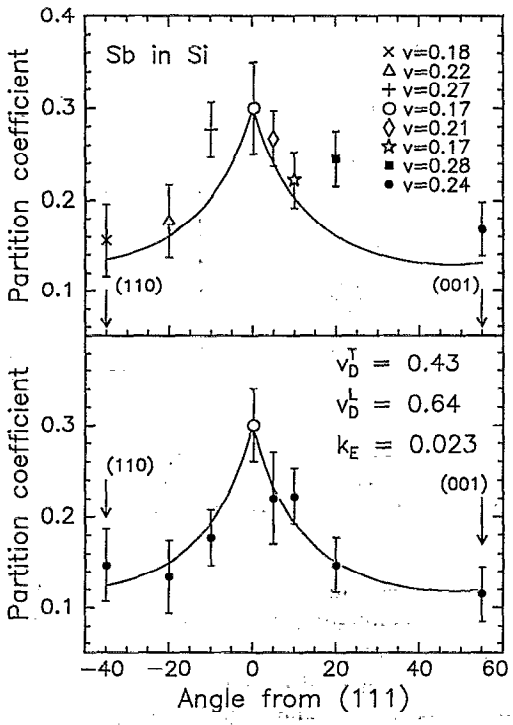

FIG. 9. Upper: Experimental data for the partition coefficient for Sb at various substrate orientations; note that each sample has solidified at a different interface velocity. Lower: same as before after the scaling all points to $v=0.17$ m/s. The solid line is calculated from Eq. (3) with the values of v_D^T, v_D^L, and k_e indicated.

2. Antimony

We used the same procedure in the case of Sb-implanted samples; the data are shown in Fig. 9(a). The Sb samples were irradiated under the same conditions used for As. The shot-to-shot variation of the measured melt duration was smaller than in the case of As, and the calculated velocities ranged only from 0.17 to 0.28 m/s. For this reason there is less scatter in the raw data. Fitting the RBS depth profiles yielded a liquid diffusion coefficient of 2×10^{-4} cm^2/s, which is slightly higher than Kodera's value[27] of 1.5×10^{-4} cm^2/s. We repeated the same scaling procedure described above, and the results are shown in Fig. 9(b): k at $v=0.17$ m/s varies from 0.15 at (110) to 0.3 at (111) and to 0.13 at (001). The fit to this data gives $v_D^T=0.43$ m/s and $v_D^L=0.64$ m/s. Iteration of the scaling procedure produced no significant change in these values.

3. Germanium

Successful fitting of the orientation dependence of the partition coefficient has been obtained for all the impurities except germanium. No evidence of anomalous behavior can be seen from the Ge depth profiles; the agreement between the measured and simulated Ge profiles was no worse than for any other impurity investigated. We measured a diffusion coefficient of 3×10^{-4} cm^2/s and k values between 0.75 and 0.85, but observed no systematic orientation dependence. From the RBS profiles we ruled out the possibility of loss of material at the surface, which would result in a higher apparent k. At present we do not have any explanation for this behavior; work is still in progress to clarify this anomaly. For completeness, the best-fit k-values for Ge in Si are given in Table IV.

IV. DISCUSSION

We have shown that the aperiodic stepwise growth model provides a very good description of partitioning of substitutional impurities in silicon. The model correctly describes the orientation dependence of k in all cases studied with the exception of Ge; it also matches the velocity-dependence of k in the two cases for which accurate measurements exist. The velocity range spanned by the entire set of experiments is about two orders of magnitude (0.1–14 m/s).

One factor limiting the utility of the ASGM is that the ledge and terrace diffusive speeds v_D^L and v_D^T have little or no relation to readily measurable physical quantities and therefore must be treated as fitting parameters. For systems in which the partition coefficient has not been or cannot be measured, there currently is no way to predict, or even to make educated guesses for, the values of these parameters.

A search was made for an empirical correlation between the diffusive speeds and other independently measurable thermophysical parameters, or combinations of them, that may in some way be representative of the driving force for partitioning or the atomic mobility. For example, White *et al.*[1] were able to correlate the maximum attainable supersaturation, but not the diffusive speed, with the covalent radius of the dopant. One possibility we investigated was that the diffusion coefficient in the solid at the melting point might represent the difficulty the solute atoms have in leaving the solid, and might therefore correlate with a diffusive speed for trapping. Dopants such as Pb and Zn are slow diffusers in Ge, but fast diffusers in Si. It has been shown[29] that at velocities of a few m/s they are trapped in Ge but show partitioning in Si, while impurities that are slow diffusers (such as Te and Sb) in both substrates are trapped in both. Similarly, the diffusion coefficient in the liquid might represent the ability of the solute to escape from the advancing interface.

It has been suggested[30] that the diffusion coefficient at the crystal/melt interface D_i should be intermediate between

TABLE IV. k for Ge in Si.

Angle	−35	−10	−5	−0.25	0	5	10	20	55
v (m/s)	0.39	0.13	0.26	0.27	0.61	0.23	0.31	0.28	0.23
k	0.68	0.67	0.69	0.74	0.76	0.69	0.66	0.62	0.7

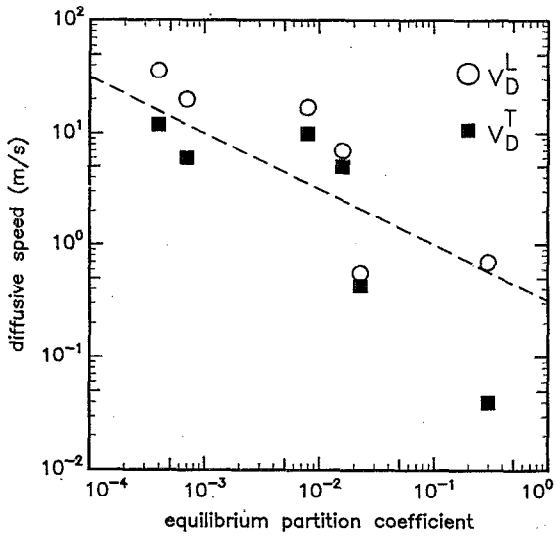

FIG. 10. Correlation between the diffusive speeds of the ASGM and the equilibrium partition coefficient.

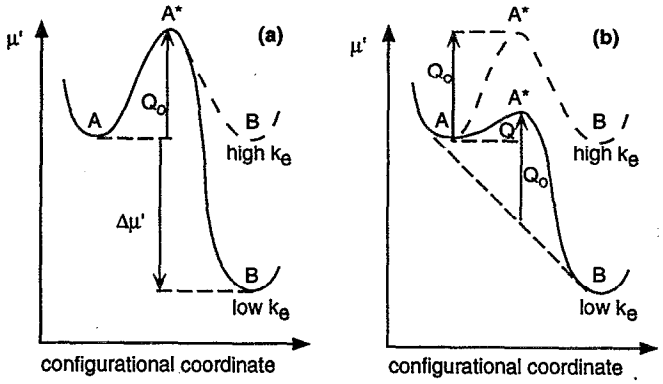

FIG. 11. Reaction coordinate diagram. In (a) the activation barrier remains a fixed height Q_0 above the initial state A, while in (b) it changes with the driving force $\Delta\mu'$, remaining a fixed height q_0 above the mean of A and B.

those of the two adjacent phases; if so, it might be given by $D_i = \sqrt{D_s D_l}$, where D_s and D_l are the diffusion coefficients in the solid and in the liquid, respectively. D_i should then be related to the interface diffusive velocity by $v_D = D_i/\lambda$, where λ is the jump distance (not[26] the interface thickness). However, none of these quantities seems to be correlated to v_D^L or v_D^T determined by fitting our solute trapping measurements, at least not in any simple way. The only quantity we have been able to correlate with the diffusive speeds is the equilibrium partition coefficient k_e. In Fig. 10 we plot the diffusive speeds determined in this work and elsewhere[16,21] versus the equilibrium partition coefficient. An inverse correlation seems to exist among these quantities. A weaker correlation might also exist with the solubility limit, although experiments have shown[31] that k_e and the solubility limit are linearly related for substitutional impurities in silicon.

The correlation presented in Fig. 10 indicates that the stronger the driving force for partitioning of solute into the liquid, the faster one must grow to trap it in the solid. Measurements of the velocity dependence of the partition coefficient in aluminum and silicon[26] have shown a similar correlation between the interface diffusive velocity v_D of the CGM model and k_e, thus supporting the correlation found here. It is perhaps not unreasonable to expect such a correlation. However, this correlation does not follow directly from the ASGM in its present form. Rather, one must consider how a change in driving force affects the solute-solvent redistribution flux.

In the ASGM (and in the CGM) solute atoms are assumed to crystallize into the lattice with the surrounding solvent atoms, and the solute subsequently attempts to escape back into the liquid. The diffusive speeds v_D^T and v_D^L originate from activation barriers (Q in Fig. 11) which must be surmounted for the solute atom to jump back into the liquid, while the equilibrium partition coefficient k_e is related to the driving force $\Delta\mu'$ for this redistribution. In the original derivation of the ASGM (and CGM), these two quantities were assumed to be independent. However, if the potential of the transition state configuration does not remain at a fixed height above the initial state A [as in Fig. 11(a)], but rather changes with the potential of the final state B [Fig. 11(b)], the diffusive speeds will appear to be related to the equilibrium partition coefficient. If a linear relation between the barrier height and the driving force is assumed:[26]

$$Q = Q_0 + \alpha\Delta\mu', \tag{6}$$

(here α is a constant between 0 and 1), the slope of a $\log v_D^L$ or $\log v_D^T$ vs $\log k_e$ plot will be $-\alpha$:

$$\log v_D^L = \log(\lambda\nu) - \frac{(Q_0 + \alpha\Delta\mu')}{RT} \tag{7}$$

$$= \log(\lambda\nu) - \frac{Q_0}{RT} - \alpha \log k_e \tag{8}$$

in which ν is an attempt frequency. The dashed line in Fig. 10 has a slope of $-1/2$ and is intended only to guide the eye and to indicate that the data are roughly consistent with $\alpha = 1/2$; the y intercept has been placed arbitrarily at -0.5. The value $\alpha = 1/2$ is selected as it corresponds to the barrier's remaining at a fixed height above the average potential of the A and B states, as depicted in Fig. 11(b). Actual least-squares fits to the data yield $\log v_D^L = -0.556 - 0.624 \log k_e$ and $\log v_D^T = -1.347$
$-0.783 \log k_e$. When the points are combined, the slope of the least-squares fitted line is -0.703.

While the correlation between diffusive speeds and k_e has been seen in metals as well as semiconductors, it remains an open question whether the crystal/melt interface is sharp enough to advance by stepwise growth in metals, and whether solute trapping behaves similarly in those systems.

V. CONCLUSION

A clear picture of solute trapping of substitutional elements in silicon has emerged. Solidification in the meter-per-second regime in Si occurs by the lateral growth of (111) terraces of unit height. For a given interface speed, the steps will be farther apart and will have to move rapidly as (111) is approached. As the step edges are atomically rough, solute is

trapped via continuous growth model kinetics, characterized by a ledge diffusive speed v_D^L. The solute incorporated into the solid by the moving step then has some time to diffuse out of the terrace back into the liquid, at speed v_D^T, before being permanently buried by the passage of the next step after a random interval. The aperiodic stepwise growth model based on this picture is a microscopic interface model that correctly describes the orientation and velocity dependence of the partition coefficient for a given species using just two parameters, the diffusive speeds v_D^T and v_D^L. Although the values of these two parameters cannot be predicted theoretically, an empirical inverse correlation has been found between the diffusive speeds and the equilibrium partition coefficient. The correlation can be rationalized by stating that the more strongly the solute atoms "want" to stay in the liquid, the faster one must solidify in order to trap them into the solid.

ACKNOWLEDGMENTS

The authors thank Michael O. Thompson for providing the original heat-flow code upon which our current simulation code is based, and David Hoglund for assisting with the heat-flow simulations. This research was supported by the U.S. Department of Energy under Grant No. DE-FG02-89ER45401. One of us (R.R.) was supported by the National Science Foundation under Grant No. DMR-92-08931.

[1] C. W. White, S. R. Wilson, B. R. Appleton, and F. W. Young, Jr., J. Appl. Phys. **51**, 738 (1980).
[2] J. C. Baker and J. W. Cahn, Acta Metall. **17**, 575 (1969).
[3] S. U. Campisano, G. Foti, P. Baeri, M. G. Grimaldi, and E. Rimini, Appl. Phys. Lett. **37**, 719 (1980).
[4] P. Baeri, S. U. Campisano, M. G. Grimaldi, and E. Rimini, in *Laser and Electron Beam Processing of Materials*, edited by C. W. White and P. S. Peercy (Academic, New York, 1980), p. 130.
[5] M. J. Aziz, J. Y. Tsao, M. O. Thompson, P. S. Peercy, and C. W. White, Phys. Rev. Lett. **56**, 2489 (1986).
[6] J. W. Cahn, S. R. Coriell, and W. J. Boettinger, in *Laser and Electron Beam Processing of Materials*, edited by C. W. White and P. S. Peercy (Academic, New York, 1980), p. 89.
[7] A. A. Chernov, in *Growth of Crystals*, edited by N. N. Sheftal (Consultants Bureau, New York, 1962), Vol. 3, p. 35.
[8] M. J. Aziz, J. Appl. Phys. **53**, 1158 (1982).
[9] K. A. Jackson, G. H. Gilmer, and H. J. Leamy, in *AIP Conference Proceedings* (AIP, New York, 1979), p. 102.
[10] K. A. Jackson, in *Surface Modification and Alloying by Laser, Ion and Electron Beams*, edited by J. M. Poate, G. Foti, and D. C. Jacobson (Plenum, New York, 1983), p. 51.
[11] C. A. MacDonald, A. M. Malvezzi, and F. Spaepen, J. Appl. Phys. **65**, 129 (1989).
[12] J. A. Kittl, M. J. Aziz, D. P. Brunco, and M. O. Thompson, J. Cryst. Growth (in press), and references therein.
[13] M. J. Aziz, J. Y. Tsao, M. O. Thompson, P. S. Peercy, and C. W. White, Mater. Res. Soc. Proc. **35**, 153 (1985).
[14] M. J. Aziz and T. Kaplan, Acta Metall. **36**, 2335 (1988).
[15] M. J. Aziz, in *Rapid Solidification Processing: Principles and Technologies III*, edited by R. Mehrabian (National Bureau of Standards, Gaithersburg, MD, 1982), p. 113.
[16] L. M. Goldman and M. J. Aziz, J. Mater. Res. **2**, 5241 (1987).
[17] M. J. Aziz, J. Y. Tsao, M. O. Thompson, P. S. Peercy, and C. W. White, Phys. Rev. Lett. **56**, 2489 (1986).
[18] P. Baeri, G. Foti, J. M. Poate, S. U. Campisano, and A. G. Cullis, Appl. Phys. Lett. **38**, 800 (1981).
[19] G. H. Gilmer, Mater. Res. Soc. Proc. **13**, 249 (1983).
[20] B. C. Larson, J. Z. Tischler, and D. M. Mills, J. Mater. Res. **1**, 144 (1986).
[21] M. J. Aziz and C. W. White, Phys. Rev. Lett. **57**, 2675 (1986).
[22] S. J. Cook and P. Clancy, J. Chem. Phys. **99**, 2192 (1993).
[23] M. J. Aziz, J. Y. Tsao, M. O. Thompson, P. S. Peercy, and C. W. White, Mater. Res. Soc. Proc. **57**, 487 (1987).
[24] M. J. Aziz, C. W. White, J. Narayan, and B. Stritzker, in *Energy Beam-Solid Interactions and Transient Thermal Processing*, edited by V. T. Nguyen and A. G. Cullis (Editions de Physique, Paris, 1985), p. 231.
[25] P. Baeri, J. M. Poate, S. U. Campisano, G. Foti, E. Rimini, and A. G. Cullis, Appl. Phys. Lett. **37**, 912 (1980).
[26] P. M. Smith and M. J. Aziz, Acta Metall. Mater. (in press).
[27] H. Kodera, Jpn. J. Appl. Phys. **2**, 212 (1963).
[28] D. E. Hoglund, M. J. Aziz, S. R. Stiffler, M. O. Thompson, J. Y. Tsao, and P. S. Peercy, J. Cryst. Growth **109**, 107 (1991).
[29] P. Baeri and A. E. Barbarino (private communication).
[30] S. U. Campisano, E. Rimini, P. Baeri, and G. Foti, Appl. Phys. Lett. **37**, 170 (1980).
[31] E. Fogarassy, R. Stuck, J. J. Grob, A. Grob, and P. Siffert, in *Laser and Electron Beam Processing of Materials*, edited by C. W. White and P. S. Peercy (Academic, New York, 1980), p. 117.
[32] M. J. Aziz, J. Y. Tsao, M. O. Thompson, P. S. Peercy, C. W. White, and W. H. Christie, Mater. Res. Soc. Proc. **35**, 135 (1985).
[33] C. W. White, B. R. Appleton, and S. R. Wilson, in *Laser Annealing of Semiconductors*, edited by J. M. Poate and J. W. Mayer (Academic, New York, 1982), p. 111.